

# Positional Isomers of Isocyanoazulenes as Axial Ligands Coordinated to Ruthenium(II) Tetraphenylporphyrin: Fine-Tuning Redox and Optical Profiles

Mahtab Fathi-Rasekh,<sup>†,¶</sup> Gregory T. Rohde,<sup>‡,¶</sup> Mason D. Hart,<sup>§</sup> Toshinori Nakakita,<sup>§</sup> Yuriy V. Zatsikha,<sup>#</sup> Rashid R. Valiev,<sup>||,⊥,¶</sup> Mikhail V. Barybin,<sup>\*,§</sup> and Victor N. Nemykin<sup>\*,†,¶</sup>

<sup>†</sup>Department of Chemistry and Biochemistry, University of Minnesota Duluth, 1039 University Drive, Duluth, Minnesota 55812, United States

<sup>‡</sup>Marshall School, Duluth, Minnesota 55811, United States

<sup>§</sup>Department of Chemistry, University of Kansas, 1567 Irving Hill Road, Lawrence, Kansas 66045, United States

<sup>||</sup>Tomsk State University, 36, Lenin Avenue, 634050 Tomsk, Russia

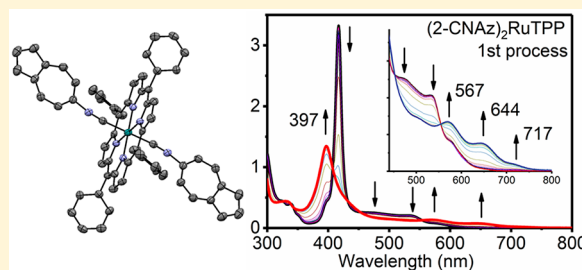
<sup>⊥</sup>University of Helsinki, P.O. Box 55, FIN-00014 Helsinki, Finland

<sup>#</sup>Department of Chemistry, University of Manitoba, 144 Dysart Road, Winnipeg, MB R3T 2N2, Canada

## Supporting Information

**ABSTRACT:** Two isomeric ruthenium(II)/5,10,15,20-tetraphenylporphyrin complexes featuring axially coordinated redox-active, low-optical gap 2- or 6-isocyanoazulene ligands have been isolated and characterized by NMR, UV–vis, and magnetic circular dichroism (MCD) spectroscopic methods, high-resolution mass spectrometry, and single-crystal X-ray crystallography. The UV–vis and MCD spectra support the presence of the low-energy, azulene-centered transitions in the Q band region of the porphyrin chromophore. The first coordination sphere in new  $L_2RuTPP$  complexes reflects compressed tetragonal geometry. The redox

properties of the new compounds were assessed by electrochemical and spectroelectrochemical means and correlated with the electronic structures predicted by density functional theory and CASSCF calculations. Both experimental and theoretical data are consistent with the first two reduction processes involving the axial azulenic ligands, whereas the oxidation profile (in the direction of increasing potential) is exerted by the ruthenium ion, the porphyrin core, and the axial azulenic moieties.



## INTRODUCTION

Organic isocyanides,  $C\equiv N-R$ , are important constituents in coordination chemistry's ligand toolbox, particularly because of their tunable steric and  $\sigma$ -donor/ $\pi$ -acceptor ratio characteristics.<sup>1–5</sup> Whereas the coordination of organic isocyanides to a variety of metalloporphyrins<sup>6–14</sup> and metallophthalocyanines<sup>15–18</sup> has been well-documented, combining redox non-innocent organic and organometallic isocyanides with such transition metal platforms offers additional distinct opportunities in the design of molecular wires.<sup>19–22</sup> Indeed, axial coordination of isocyanoferrrocene and 1,1'-diisocyanoferrrocene<sup>23</sup> to Ru(II)porphyrins and phthalocyanines has been recently shown to exert unusual redox profiles of the corresponding adducts that are attractive in the context of applications in molecular electronics, including molecular wires.<sup>24,25</sup> Isocyanoazulenes<sup>26</sup> constitute a special class of isocyanoarenes and feature the non-benzenoid aromatic substituent comprising fused five- and seven-membered  $sp^2$ -carbon rings. The polar nature of the azulenic scaffold (ca. 1.0 D) and the position of its attachment to the isocyanide junction allow the electronic structure of transition metal–isocyanide

complexes to be manipulated.<sup>26</sup> In order to expand the potential utility of isocyanoazulenes in assembling organometallic molecular wires,<sup>27,28</sup> herein we consider two isomeric systems involving either 2-isocyanoazulene (2-CNAz) or 6-isocyanoazulene (6-CNAz) ligands axially coordinated to the ruthenium(II) tetraphenylporphyrin (TPP) core (Scheme 1). The choice of this isomeric pair stemmed, in part, from the opposite orientation of the azulenic dipole in the isocyanoazulene ligands. The physicochemical characteristics of the new complexes  $L_2RuTPP$  ( $L = 2$ - or 6-isocyanoazulene) are compared to those of other previously reported  $(RNC)_2RuTPP$  compounds.<sup>29–32</sup>

## RESULTS AND DISCUSSION

### Synthetic, Spectroscopic, and Crystallographic Work.

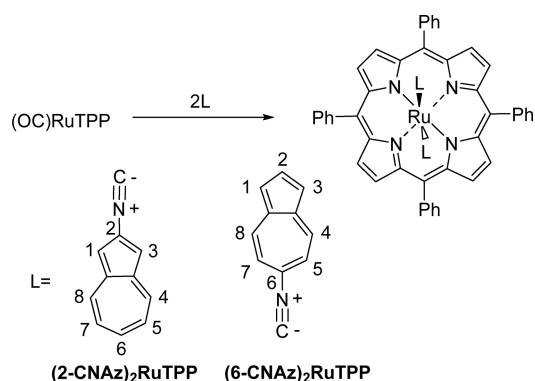
The isocyanoazulene complexes  $(2-CNAz)_2RuTPP$  and  $(6-CNAz)_2RuTPP$  were accessed using a simple coordination reaction shown in Scheme 1.

Received: April 9, 2019

Published: June 26, 2019



### Scheme 1. Synthetic Strategy for the Preparation of the (RNC)<sub>2</sub>RuTPP Complexes



Similar to the <sup>1</sup>H NMR patterns documented for other axially coordinated diamagnetic ruthenium/iron porphyrins and phthalocyanines,<sup>33–39</sup> the <sup>1</sup>H NMR resonances corresponding to the axial ligands (i.e., the isocyanoozulenyls) in (2-CNAz)<sub>2</sub>RuTPP and (6-CNAz)<sub>2</sub>RuTPP are shifted significantly upfield compared to the corresponding free ligands. Both isomeric complexes give rise to the same number of <sup>1</sup>H resonances with four signals attributable to the porphyrin macrocycle (thereby indicating a pseudo-*D*<sub>4h</sub> symmetry with free rotation about the C–Ru–C axis) and four signals corresponding to two equivalent azulenylyl moieties. Notably, the <sup>1</sup>H NMR signatures of the tetraphenylporphyrin cores in (2-CNAz)<sub>2</sub>RuTPP and (6-CNAz)<sub>2</sub>RuTPP are very similar to those previously documented for other L<sub>2</sub>RuTPP complexes.<sup>24</sup>

The <sup>1</sup>H NMR patterns for the axial isocyanoozulenyl ligands are markedly different for the two isomers.<sup>26</sup> For complex (2-CNAz)<sub>2</sub>RuTPP, the <sup>1</sup>H NMR resonance for the H atoms at 1,3-positions of the azulenic scaffold (H<sup>1,3</sup>) is shifted –1.96 ppm (upfield), whereas the H<sup>4,8</sup> signal is shifted –1.43 ppm (upfield), compared to the corresponding resonances documented for the H<sup>1,3</sup> and H<sup>4,8</sup> nuclei of the free 2-CNAz ligand dissolved in the same solvent. The relatively large upfield shift of the H<sup>1,3</sup> resonance is consistent with the closer proximity of these azulenic H atoms to the porphyrin ring. For the (6-CNAz)<sub>2</sub>RuTPP complex, the situation is reversed. Indeed, the <sup>1</sup>H NMR signal for the H<sup>5,7</sup> nuclei is shifted –2.62 ppm, whereas that for the H<sup>4,8</sup> nuclei is shifted –0.87 ppm, compared to the corresponding resonances recorded for the free 6-CNAz ligand dissolved in the same solvent. In agreement with the previous argument, the H<sup>5,7</sup> azulenic nuclei in (6-CNAz)<sub>2</sub>RuTPP are positioned closer to the porphyrin ring and, therefore, exhibit an upfield shift of the corresponding <sup>1</sup>H NMR resonances that is larger than that of the H<sup>1,3</sup> environment. Moreover, the <sup>1</sup>H NMR resonance for the H<sup>5,7</sup> atoms of 6-CNAz undergoes an upfield shift (–2.62 ppm) upon coordination to form (6-CNAz)<sub>2</sub>RuTPP greater than the upfield shift (–1.96 ppm) of the <sup>1</sup>H NMR signal for the H<sup>1,3</sup> atoms of 2-CNAz upon coordination of the latter to form (2-CNAz)<sub>2</sub>RuTPP. This observation is consistent with the azulenic H<sup>5,7</sup> atoms in the (6-CNAz)<sub>2</sub>RuTPP complex being in closer proximity to the porphyrin ring as compared to the azulenic H<sup>1,3</sup> nuclei in the (2-CNAz)<sub>2</sub>RuTPP complex. The single-crystal X-ray structural analyses of (2-CNAz)<sub>2</sub>RuTPP and (6-CNAz)<sub>2</sub>RuTPP confirm the above statement (vide infra). The C≡N stretching vibrations (ν<sub>CN</sub>) of the isocyanoo junctions in (2-CNAz)<sub>2</sub>RuTPP and (6-CNAz)<sub>2</sub>RuTPP complexes occur at 2067 and 2061 cm<sup>–1</sup>,

respectively. Notably, the ν<sub>CN</sub> bands in the IR spectra of the free 2-CNAz and 6-CNAz ligands are at 2118 and 2111 cm<sup>–1</sup>, respectively.<sup>26</sup> The depressions in ν<sub>CN</sub> energy upon coordination of 2-CNAz or 6-CNAz to RuTPP are nearly identical (51 cm<sup>–1</sup> vs 50 cm<sup>–1</sup>) and signify appreciable Ru(*dπ*) → CNAz(*pπ*<sup>\*</sup>) backbonding interactions within (2-CNAz)<sub>2</sub>RuTPP and (6-CNAz)<sub>2</sub>RuTPP complexes.<sup>1</sup> Similar shifts for (AzNC)<sub>6</sub>Cr and (RNC)<sub>2</sub>RuTPP systems were reported earlier.<sup>24,26</sup> The APCI mass spectra of (2-CNAz)<sub>2</sub>RuTPP and (6-CNAz)<sub>2</sub>RuTPP are illustrated in the Supporting Information and confirm the 2:1 isocyanoozulenyl/ruthenium porphyrin core stoichiometry in these adducts.

The UV–vis and magnetic circular dichroism (MCD) spectra of the complexes (2-CNAz)<sub>2</sub>RuTPP and (6-CNAz)<sub>2</sub>RuTPP are shown in Figure 1. As in the case of the previously reported

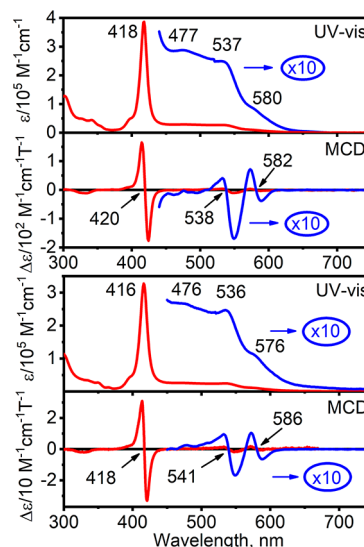


**Figure 1.** Experimental UV–vis and MCD spectra of (2-CNAz)<sub>2</sub>RuTPP (top) and (6-CNAz)<sub>2</sub>RuTPP (bottom).

(RNC)<sub>2</sub>RuTPP complexes,<sup>24,29,30,32</sup> these spectra essentially constitute the superposition of the corresponding spectra recorded for RuTPP and the axial ligands, complemented by the additional ruthenium to isocyanoozulenyl (metal to ligand) charge transfer transitions. Given that the intensities and energies of the π–π<sup>\*</sup> transitions for both azulenic moieties and the TPP fragments in the Q band region are similar, the UV–vis spectra of **1** and **2** are much less defined compared to the reference complex (*t*-BuNC)<sub>2</sub>RuTPP, for which clear Q<sub>0–0</sub> and Q<sub>0–1</sub> bands were observed at 582 and 529 nm, respectively.<sup>24,30</sup> However, as MCD intensities of the Faraday *B* terms for the axially coordinated isocyanoozulenyls are incomparably smaller than the *A* term intensities of the Q<sub>0–0</sub> and Q<sub>0–1</sub> bands for the TPP core, MCD spectroscopy allows unambiguous identification of the Q<sub>0–0</sub> band at 582 nm ((2-CNAz)<sub>2</sub>RuTPP) or 586 nm ((6-CNAz)<sub>2</sub>RuTPP) nm and Q<sub>0–1</sub> band at 538 nm ((2-CNAz)<sub>2</sub>RuTPP) and 541 nm ((6-CNAz)<sub>2</sub>RuTPP) nm (Figure 1). As expected for the effective four-fold symmetry of the porphyrin core in the (CNAz)<sub>2</sub>RuTPP complexes, ΔHOMO > ΔLUMO (ΔHOMO is the energy difference between the two highest-energy, TPP-centered π-orbitals, and ΔLUMO is the energy difference between the two lowest-energy, TPP-centered π<sup>\*</sup>-orbitals), which is reflected in negative-to-positive (in ascending energy) sequence of the MCD signals.<sup>40–44</sup> The Soret band

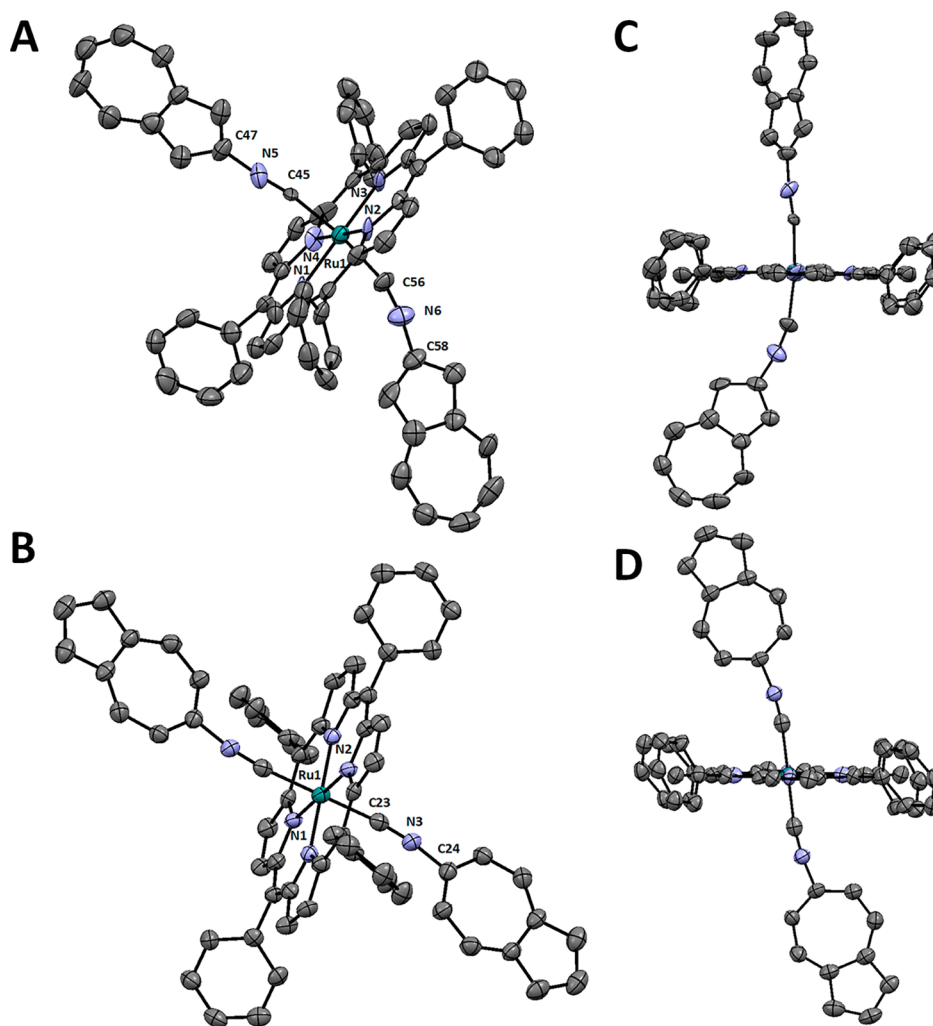


**Figure 2.** Molecular structures (A,B) and bent profiles (C,D) of  $(2\text{-CNaz})_2\text{RuTPP}$  (A,C) and  $(6\text{-CNaz})_2\text{RuTPP}$  (B,D) featuring 50% thermal ellipsoids. All hydrogen atoms are omitted for clarity, as are the toluene solvent molecules of crystallization observed in the unit cells of both  $(2\text{-CNaz})_2\text{RuTPP}$  and  $(6\text{-CNaz})_2\text{RuTPP}$ . Carbon atoms are gray, nitrogen atoms are blue, and ruthenium atoms are cyan. Selected bond distances (Å) and angles (deg):  $(6\text{-CNaz})_2\text{RuTPP}$  Ru1–C23 1.980(7), Ru1–N1 2.064(5), Ru1–N2 2.054(5), N3–C23 1.169(7), N3–C24 1.411(7), C23–Ru1–C23 180.0, C23–N3–C24 171.3(6), N3–C23–Ru1 171.3(5);  $(2\text{-CNaz})_2\text{RuTPP}$  Ru1–N1 2.095(11), Ru1–N2 2.071(10), Ru1–N3 2.103(10), Ru1–N4 2.063(9), Ru1–C45 1.999(11), Ru1–C56 1.995(13), N5–C45 1.150(16), N5–C47 1.391(17), N6–C56 1.167(17), N6–C58 1.382(18), C45–Ru1–C56 172.1(6), C45–N5–C47 173.4(15), C56–N6–C58 169.3(16), Ru1–C56–N6 164.0(14), Ru1–C45–N5 171.6(11), C45–N5–C47 173.4(15), C56–N6–C58 169.3(16).

region in the electronic spectra of the  $(\text{CNaz})_2\text{RuTPP}$  complexes is dominated by a single band observed at ca. 417 nm, which is associated with a very intense Faraday A term in the corresponding MCD spectra (Figure 1). More importantly, a very small intensity of the MCD signals between 450 and 500 nm, which is associated with fairly intense UV–vis transitions in this region, suggests the presence of either azulene-centered  $\pi\text{-}\pi^*$  or ruthenium-to-azulene charge-transfer transitions in this spectral envelope.

The molecular structures of  $(2\text{-CNaz})_2\text{RuTPP}$  and  $(6\text{-CNaz})_2\text{RuTPP}$  were determined by single-crystal X-ray diffraction. Slow evaporation of a toluene solution of  $(2\text{-CNaz})_2\text{RuTPP}$  or  $(6\text{-CNaz})_2\text{RuTPP}$  at room temperature provided crystals suitable for X-ray analysis. Both  $(2\text{-CNaz})_2\text{RuTPP}$  and  $(6\text{-CNaz})_2\text{RuTPP}$  cocrystallized with one toluene molecule in the asymmetric unit. The crystal sizes were quite small, which resulted in a limited resolution of 0.90 and 0.84 Å for  $(2\text{-CNaz})_2\text{RuTPP}$  and  $(6\text{-CNaz})_2\text{RuTPP}$ , respectively. The ORTEP diagrams of  $(2\text{-CNaz})_2\text{RuTPP}$  and

$(6\text{-CNaz})_2\text{RuTPP}$  are displayed in Figure 2. Despite the low resolution of the X-ray structure for the  $(2\text{-CNaz})_2\text{RuTPP}$  complex, the structural differences between the isolated isomeric  $(2\text{-CNaz})_2\text{RuTPP}$  and  $(6\text{-CNaz})_2\text{RuTPP}$  species can be readily appreciated.

$(2\text{-CNaz})_2\text{RuTPP}$  and  $(6\text{-CNaz})_2\text{RuTPP}$  crystallize in the space groups  $P2_1/c$  and  $C2/c$ , respectively. The ruthenium ion in  $(6\text{-CNaz})_2\text{RuTPP}$  is located at the inversion center, resulting in one-half of the molecule being crystallographically unique. The Ru center sits in the plane of the porphyrin ring in both  $(2\text{-CNaz})_2\text{RuTPP}$  and  $(6\text{-CNaz})_2\text{RuTPP}$  and features a slightly compressed tetragonal environment. Consistent with the metric data reported earlier for other Ru–porphyrin–isocyanide complexes, the Ru–N bond is about 0.08 Å longer than the Ru–C distances.<sup>24,30</sup> The Ru–C distances of 1.98–1.99 Å observed for  $(2\text{-CNaz})_2\text{RuTPP}$  and  $(6\text{-CNaz})_2\text{RuTPP}$  are very similar to those previously determined for the Ru–porphyrin complexes with benzenoid isocyanoarene and isocyanoferrrocene axial ligands.<sup>24,30</sup> The isocyanide  $\text{C}\equiv\text{N}$  bond distances in

(2-CNAz)<sub>2</sub>RuTPP and (6-CNAz)<sub>2</sub>RuTPP (1.15–1.17 Å) are similar to those documented for many uncomplexed isocyanarenes, thereby suggesting a modest extent of Ru(dπ) → CNAz(pπ\*) backbonding, which is essentially counterbalanced by the C≡N bond strengthening via the AzNC → Ru σ-bonding interaction.<sup>1</sup>

**Redox Properties.** The redox properties of the azulene-containing (2-CNAz)<sub>2</sub>RuTPP and (6-CNAz)<sub>2</sub>RuTPP complexes were investigated by electrochemical and spectroelectrochemical approaches. The cyclic voltammetry (CV) and differential pulse voltammetry (DPV) profiles for the two isomers are shown in Figure 3 and numerically summarized in

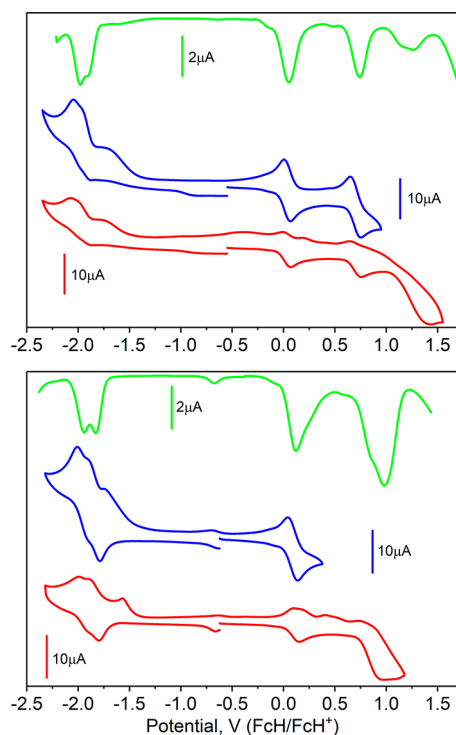


**Figure 3.** DPV (green) and CV (blue and red) electrochemical profiles for (2-CNAz)<sub>2</sub>RuTPP (top) and (6-CNAz)<sub>2</sub>RuTPP (bottom) complexes in DCM/0.05 M TFAB solution.

**Table 1.** In both cases, the first oxidation event has been assigned to the Ru<sup>II</sup>/Ru<sup>III</sup> redox couple based on the redox potential value, spectroelectrochemical data, and the electron paramagnetic resonance signatures of the previously reported<sup>29,30</sup> similar [(RNC)<sub>2</sub>RuTPP]<sup>+</sup> complexes.<sup>24,30,32</sup> As expected for (RNC)<sub>2</sub>RuTPP complexes, the Ru<sup>II</sup>/Ru<sup>III</sup> oxidation potential depends slightly on the nature of the axial ligand. Indeed, the (6-

CNAz)<sub>2</sub>RuTPP complex is about 40 mV harder to oxidize compared to the (2-CNAz)<sub>2</sub>RuTPP complex. The second reversible oxidation wave for (2-CNAz)<sub>2</sub>RuTPP, observed at 740 mV, was assigned to the oxidation of the porphyrin core, and two closely spaced irreversible processes observed at 1.14 and 1.27 V were assigned to the oxidation of the axial isocyanazulene ligands (irreversible oxidation of free 2-isocyanazulene occurs at 0.92 V).<sup>26</sup> In the case of (6-CNAz)<sub>2</sub>RuTPP, however, the irreversible oxidation potentials of the axial isocyanazulene ligands were found to be close to the reversible oxidation potential of porphyrin, and thus the second wave observed in the electrochemical experiments consists of three closely spaced single-electron electrochemical events. Two clearly observed irreversible oxidation processes involving the axial ligands of (2-CNAz)<sub>2</sub>RuTPP dissolved in dichloromethane (DCM)/0.05 M TFAB (tetrabutylammonium tetrakis(pentafluorophenyl)borate) allowed the value of the comproportionation constant for the formation of the putative mixed-valence [(2-CNAz)<sub>2</sub>RuTPP]<sup>3+</sup> complex to be estimated ( $K_c = 159$ ). However, given the irreversible nature of the axial ligand oxidation, spectroscopic documentation of the above mixed-valence species remains elusive. The CV and DPV profiles of the (CNAz)<sub>2</sub>RuTPP complexes indicate two closely spaced, partially reversible reduction events (Figure 3). Based on the similarities of observed reduction potentials to those documented for the free isocyanazulenes (Table 1),<sup>26</sup> we assigned both processes to the sequential reduction of the axial ligands. Again, although comproportionation constants for the mixed-valence [(2-CNAz)<sub>2</sub>RuTPP]<sup>-</sup> and [(6-CNAz)<sub>2</sub>RuTPP]<sup>-</sup> complexes ( $K_c = 15$  and 72, respectively) can be estimated from the electrochemical data, limited stability of these mixed-valence species under spectroelectrochemical conditions precluded their further spectroscopic characterization. Although not surprising, such behavior is in stark contrast with the other L<sub>2</sub>RuTPP complexes for which only porphyrin-centered reduction processes were observed. Overall, unlike the ruthenium porphyrins with axially coordinated isocyanoferrrocene ligands, the axially coordinated isocyanazulenes show redox activity in both oxidation and reduction directions.

In order to confirm the tentative assignments of the oxidation waves observed in electrochemical experiments, spectroelectrochemical assessment of both 2- and 6-isocyanazulene complexes was performed. During the first oxidation process under spectroelectrochemical conditions, the Soret band undergoes intensity depletion by ~60% and higher energy shift to 396–397 nm. In the Q band region, upon the first oxidation process, three new bands at ~570, 644, and ~715 nm appear in the UV–vis spectra of [(2-CNAz)<sub>2</sub>RuTPP]<sup>+</sup> and [(6-CNAz)<sub>2</sub>RuTPP]<sup>+</sup> (Figures 4 and 5). A similar transformation

**Table 1. Oxidation Potentials (V) for (RNC)<sub>2</sub>RuTPP Complexes Determined by CV and DPV in the DCM/0.05 M TFAB System at Room Temperature<sup>a</sup>**

complex	Ru <sup>II</sup> /Ru <sup>III</sup>	TPP <sup>2-</sup> /TPP <sup>-</sup>	2L/2L <sup>+</sup>	2L <sup>+</sup> /2L <sup>2+</sup>	2L/2L <sup>-</sup>	2L <sup>-</sup> /2L <sup>2-</sup>
(2-CNAz) <sub>2</sub> RuTPP	0.05	0.74	1.14 <sup>d</sup>	1.27 <sup>d</sup>	-1.91 <sup>d</sup>	-1.98 <sup>d</sup>
(6-CNAz) <sub>2</sub> RuTPP	0.09	0.84 <sup>e</sup>	0.98 <sup>d,e</sup>	0.98 <sup>d,e</sup>	-1.83 <sup>d</sup>	-1.94 <sup>d</sup>
( <i>t</i> -BuNC) <sub>2</sub> RuTPP <sup>b</sup>	-0.023	0.713				
(FcNC) <sub>2</sub> RuTPP <sup>b</sup>	0.033	0.997	0.437	0.533		
2-CNAz <sup>c</sup>			0.92 <sup>d</sup>		-1.80 <sup>d</sup>	
6-CNAz <sup>c</sup>					-1.79	

<sup>a</sup>All potentials are referenced to the FcH/FcH<sup>+</sup> couple and are ±10 mV; L is the organic isocyanide ligand. <sup>b</sup>From ref 24. <sup>c</sup>From ref 26. <sup>d</sup>Irreversible or partially reversible. <sup>e</sup>Three single-electron, closely spaced oxidation waves.

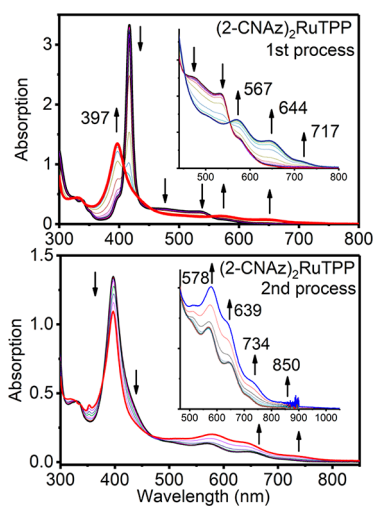


**Figure 4.** Spectroelectrochemical oxidation of the  $(2\text{-CNAz})_2\text{RuTPP}$  complex in DCM/0.15 M TFAB solution at room temperature. The first oxidation process was monitored between 0 and +0.5 V, and the second oxidation process was monitored between +0.5 and +0.9 V.

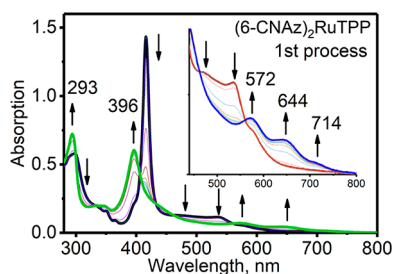


**Figure 5.** Spectroelectrochemical oxidation of the  $(6\text{-CNAz})_2\text{RuTPP}$  complex in DCM/0.15 M TFAB solution at room temperature. The first oxidation process was monitored between 0 and +0.5 V.

has already been observed in the case of the Ru–porphyrins axially coordinated with other organic isocyanide ligands, which is characteristic of the formation of  $\text{Ru}^{\text{III}}$ -porphyrins.<sup>24,29,30</sup> Because of the closeness of the porphyrin- and azulene-based oxidation potentials for  $(6\text{-CNAz})_2\text{RuTPP}$ , we did not pursue further chemical oxidation of  $[(6\text{-CNAz})_2\text{RuTPP}]^+$  to  $[(6\text{-CNAz})_2\text{RuTPP}]^{2+}$ . However, in the case of the  $(2\text{-CNAz})_2\text{RuTPP}$  complex, the first and second oxidation waves are well-separated, and thus, we were able to further oxidize the  $[(2\text{-CNAz})_2\text{RuTPP}]^+$  complex to  $[(2\text{-CNAz})_2\text{RuTPP}]^{2+}$  (Figure 4). During the second oxidation step, the intensity of the Soret band at 397 nm decreases with concomitant appearance of the new bands at 578, 639, 734, and  $\sim 850$  nm in the UV–vis–NIR spectrum. The formation of broad, low-intensity bands at ca. 850 nm is a signature indicator for the formation of a delocalized porphyrin cation radical. We also were able to effect the first oxidation process using chemical oxidation of the neutral complexes with “magic blue” radical as an oxidant (Supporting Information). The observed changes in the UV–vis spectra of  $(2\text{-CNAz})_2\text{RuTPP}$  and  $(6\text{-CNAz})_2\text{RuTPP}$  correlate well with the corresponding spectroelectrochemical data and suggest the  $\text{Ru}^{\text{II}}/\text{Ru}^{\text{III}}$  oxidation process. Overall, the spectroelectrochemical and chemical oxidation data confirm our tentative electrochemical assignments and echo the previous reports on the ruthenium(II) tetraphenylporphyrin complexes axially coordinated with organic isocyanides.

**Density Functional Theory (DFT) and Time-Dependent Density Functional Theory (TDDFT) Calculations.** The DFT-predicted frontier molecular orbitals, energy diagram, and molecular orbital compositions for  $(2\text{-CNAz})_2\text{RuTPP}$  and  $(6\text{-CNAz})_2\text{RuTPP}$  are shown in Figures 6 and 7 and Table 2. The

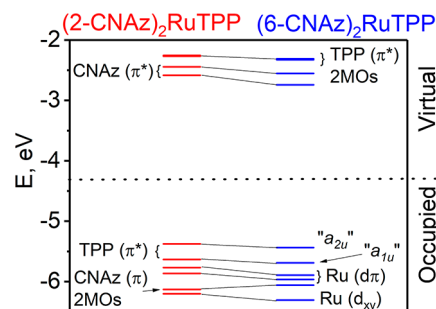


**Figure 6.** DFT-predicted orbital energy diagram for the  $(\text{AzNC})_2\text{RuTPP}$  complexes.

choice of the M06 exchange–correlation functional<sup>45</sup> for the energy and excited-state calculations was dictated by the best agreement between the theory and experiment obtained in the TDDFT calculations although the other tested exchange–correlation functionals (BP86,<sup>46,47</sup> TPSSH,<sup>48</sup> B3LYP,<sup>49</sup> CAM-B3LYP,<sup>50</sup> M06L,<sup>45</sup> M11,<sup>51</sup> MN12SX,<sup>52</sup> and M11L<sup>51</sup>) predict qualitatively similar electronic structures of the analyzed compounds. The large contribution of the Hartree–Fock exchange part in the M06 exchange–correlation functional, however, resulted in a relatively strong stabilization of the metal-centered orbitals compared to the porphyrin  $\pi$ -orbitals. Indeed, in the case of the  $(2\text{-CNAz})_2\text{RuTPP}$  and  $(6\text{-CNAz})_2\text{RuTPP}$  complexes, the HOMO and HOMO–1 were predicted to be porphyrin-centered MOs followed by the predominantly Ru-centered  $d_\pi$  molecular orbitals (HOMO–2 and HOMO–3). The difference between the TPP-centered HOMO and the primarily Ru-centered HOMO–2 was predicted to be about 0.4 eV in energy. For both complexes, DFT predicts the predominantly ruthenium-centered  $d_{xy}$ -orbital as HOMO–6. In addition, the azulene-centered, occupied molecular orbitals were found to be the HOMO–4 and HOMO–5 for both complexes. The M06 calculations correctly predict that the LUMO and LUMO+1 for  $(2\text{-CNAz})_2\text{RuTPP}$  and  $(6\text{-CNAz})_2\text{RuTPP}$  are azulene-centered, whereas the classic Gouterman’s porphyrin-centered orbitals should be the LUMO+2 and LUMO+3. Although the electrochemical experiments discussed above suggest the first oxidation event to be Ru-centered, all tested exchange–correlation functionals still predict the HOMO to be porphyrin-centered. In order to reconcile this discrepancy between the theory and experiment, we subjected the complexes to the CASSCF calculations discussed below. Overall, the DFT-predicted electronic structures of the  $(2\text{-CNAz})_2\text{RuTPP}$  and  $(6\text{-CNAz})_2\text{RuTPP}$  complexes suggest that, in addition to the classic porphyrin-centered Gouterman’s  $\pi$ – $\pi^*$  transitions, the low-energy azulene-centered  $\pi$ – $\pi^*$  transitions,<sup>53</sup> porphyrin( $\pi$ )–azulene( $\pi^*$ ) charge-transfer transitions, Ru( $d$ )–azulene( $\pi^*$ ) charge-transfer transitions, and Ru( $d$ )–porphyrin( $\pi^*$ ) charge-transfer transitions might complicate the visible region of the UV–vis spectra of  $(2\text{-CNAz})_2\text{RuTPP}$  and  $(6\text{-CNAz})_2\text{RuTPP}$ .

Indeed, the TDDFT calculations predict that the porphyrin-centered Q bands that are dominated by the single-electron HOMO, HOMO–1  $\rightarrow$  LUMO+2, LUMO+3 excitations would

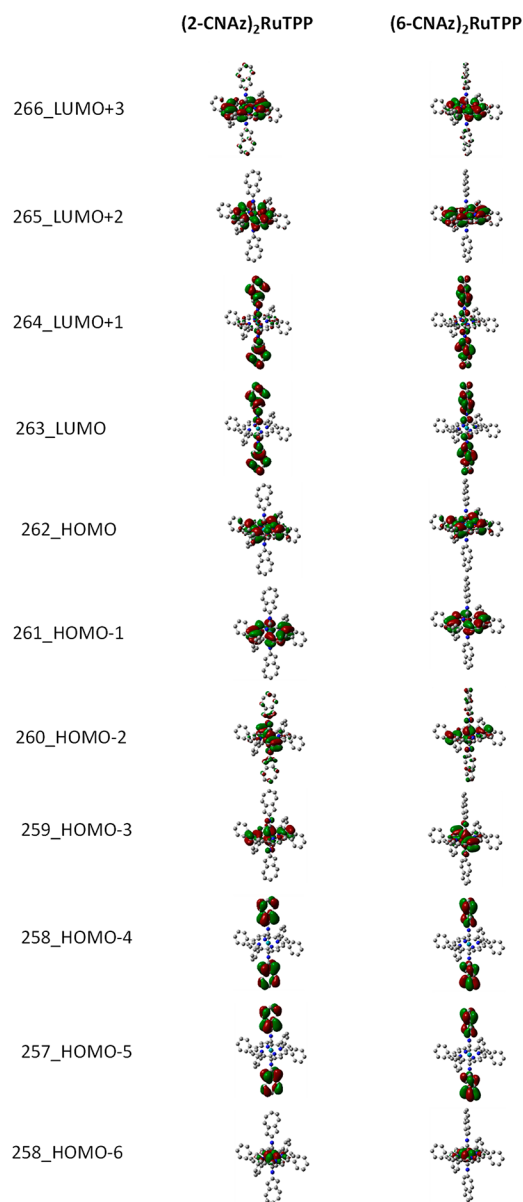


**Figure 7.** DFT-predicted frontier orbitals for the  $(\text{AzNC})_2\text{RuTPP}$  complexes.

be observed at ca. 550 nm (labeled as “TPP” in Figure 8). The TDDFT analysis also predicts several low-energy, predominantly azulene-based transitions HOMO–4, HOMO–5  $\rightarrow$  LUMO, LUMO+1 in the Q band region, with one having an intensity comparable to those of the porphyrin core-centered Q bands (labeled as “Az” in Figure 8). The TDDFT-predicted energies of the latter (528 nm for  $(2\text{-CNAz})_2\text{RuTPP}$  and 576 nm for  $(6\text{-CNAz})_2\text{RuTPP}$ ) follow the trend observed for the free isocyanazulene ligands. Our TDDFT calculations predict several porphyrin ( $\pi$ )  $\rightarrow$  azulene ( $\pi^*$ ) transitions in the Q band region, but those should have very low intensities. In contrast, the TDDFT-predicted intensity for the predominantly  $\text{Ru}(d\pi) \rightarrow$  azulene ( $\pi^*$ ) band (predicted at 483 nm for  $(2\text{-CNAz})_2\text{RuTPP}$  and 502 nm for  $(6\text{-CNAz})_2\text{RuTPP}$ ) is quite large (labeled as “Ru  $\rightarrow$  Az” in Figure 8). These transitions are responsible for the broad absorption observed in the UV–vis spectra of  $(\text{CNAz})_2\text{RuTPP}$  complexes between 450 and 500 nm. The most intense band predicted by the TDDFT calculations for the azulene-containing metalloporphyrin complexes is

**Table 2.** DFT-Predicted Molecular Orbital Compositions for the  $(\text{AzNC})_2\text{RuTPP}$  Complexes<sup>a</sup>

$(2\text{-CNAz})_2\text{RuTPP}$ composition, %					
MO	energy (eV)	symmetry	Ru	porphyrin	2-CNAz
256	–6.201	$a_g$	88.84	11.09	0.07
257	–6.129	$a_u$	0	0.08	99.92
258	–6.129	$a_g$	0.11	0.2	99.69
259	–5.865	$a_g$	59.87	34.68	5.45
260	–5.769	$a_g$	58.37	28.89	12.74
261	–5.634	$a_u$	0.02	99.97	0.01
262	–5.377	$a_u$	<b>0.29</b>	<b>97.49</b>	<b>2.22</b>
263	–2.583	$a_u$	<b>0.92</b>	<b>7.15</b>	<b>91.93</b>
264	–2.443	$a_g$	1.78	12.83	85.39
265	–2.269	$a_g$	5.07	94.36	0.57
266	–2.255	$a_g$	6.89	85.54	7.57
$(6\text{-CNAz})_2\text{RuTPP}$ composition, %					
MO	energy (eV)	symmetry	Ru	porphyrin	6-CNAz
256	–6.305	$a_g$	88.85	11.12	0.03
257	–6.059	$a_u$	0.02	0.15	99.83
258	–6.059	$a_g$	0	0.08	99.92
259	–5.964	$a_g$	57.48	34.63	7.89
260	–5.892	$a_g$	57.39	31.13	11.49
261	–5.69	$a_u$	0.02	99.95	0.03
262	–5.438	$a_u$	<b>0.28</b>	<b>95.75</b>	<b>3.97</b>
263	–2.742	$a_u$	<b>1.26</b>	<b>3.87</b>	<b>94.87</b>
264	–2.554	$a_g$	3.17	8.44	88.39
265	–2.326	$a_g$	4.89	93.91	1.2
266	–2.312	$a_g$	7.07	86.59	6.34
282	0.898	$a_g$	10.13	6.61	83.25

<sup>a</sup>HOMO and LUMO are indicated in bold. Both complexes were optimized in the  $C_i$  point group.

located at 409 nm for both complexes and is dominated by the classic Gouterman’s<sup>54,55</sup> porphyrin-centered, HOMO, HOMO–1  $\rightarrow$  LUMO+2, LUMO+3 single-electron excitations. Thus, the TDDFT analysis of the UV–vis profile of the azulene-containing metalloporphyrin complexes discussed herein is in reasonable agreement with the corresponding experimental data and explains the broadening of the Q band region for these systems. In particular, TDDFT accurately predicted energies and relative intensities of the porphyrin-centered Q and Soret bands as well as azulene-centered  $\pi$ – $\pi^*$  transitions. However, although TDDFT-predicted energies of the charge-transfer transitions were in reasonable agreement with the experimental data, their oscillator strengths were clearly overestimated.

The results of the CASSCF calculations employing the XMC-QDPT2 approach are illustrated in Figure 9. When we take into consideration a high computational cost, only  $(2\text{-CNAz})_2\text{RuTPP}$  was treated at this level of theory. In contrast to the DFT results, the XMC-QDPT2 calculations indicate that the HOMO is completely localized with the ruthenium’s  $d_{xy}$ -orbital, which is in better agreement with the electrochemical and spectroelectrochemical experiments. According to the XMC-QDPT2 calculations, the energy of the  $S_0 \rightarrow S_1$  transition is 1.7 eV (or 729 nm), and its oscillator strength is 0.009 (the oscillator strength of this transition is comparable to that predicted by TDDFT). It constitutes a charge transfer from the ruthenium-based HOMO ( $4d_{xy}$ -orbital) to the porphyrin-centered LUMO+3. Notably, the weight of the HOMO  $\rightarrow$

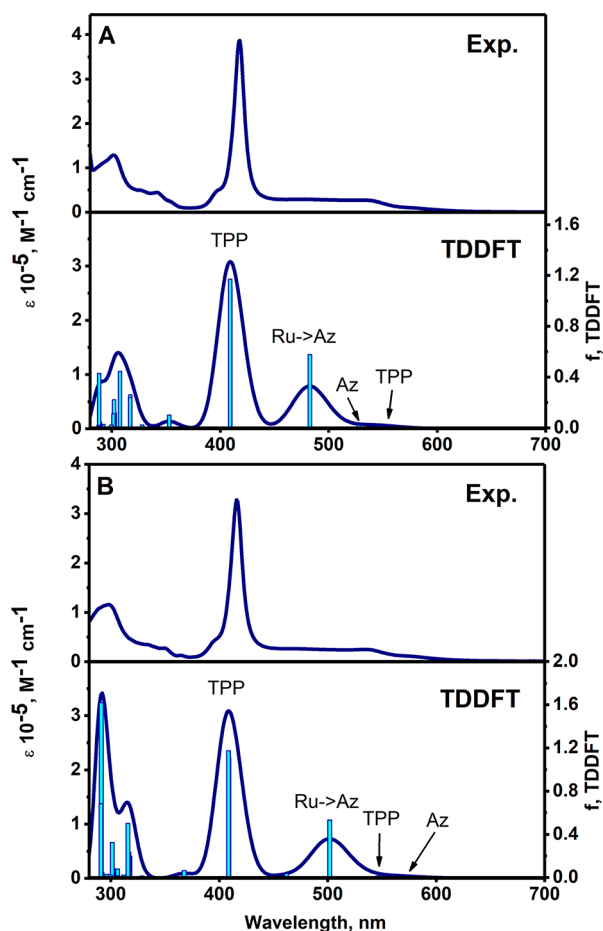


**Figure 8.** Experimental UV-vis (top) and TDDFT-predicted (bottom) spectra of (2-CNaz)<sub>2</sub>RuTPP (A) and (6-CNaz)<sub>2</sub>RuTPP (B).

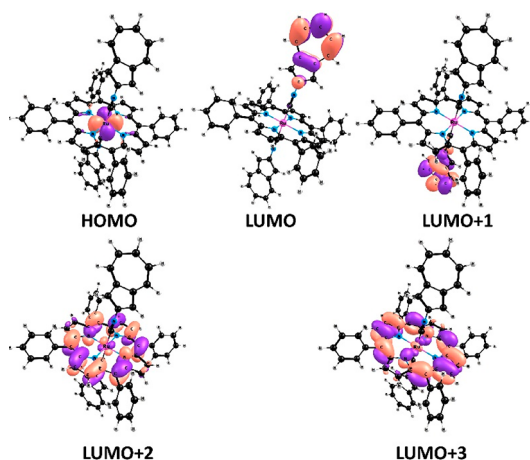


**Figure 9.** CASSCF-generated frontier MOs for (2-CNaz)<sub>2</sub>RuTPP. The  $S_0 \rightarrow S_1$  event corresponds to the electronic transition from HOMO to LUMO+3 with the weight of 0.64.

LUMO, HOMO  $\rightarrow$  LUMO+1 for  $S_0 \rightarrow S_1$  transition does not exceed 0.1.

## CONCLUSIONS

Two new complexes featuring the ruthenium(II) tetraphenylporphyrin core axially coordinated with a pair of 2- or 6-isocyanoazulene ligands ((2-CNaz)<sub>2</sub>RuTPP and (6-

CNaz)<sub>2</sub>RuTPP) were isolated, and their physicochemical profiles were interrogated using UV-vis, MCD, NMR, and IR spectroscopies as well as by ESI-MS spectrometry and X-ray crystallography. The redox properties of (2-CNaz)<sub>2</sub>RuTPP and (6-CNaz)<sub>2</sub>RuTPP were probed using electrochemical (CV and DPV), spectroelectrochemical, and chemical oxidation methods and correlated with those documented earlier for other (RNC)<sub>2</sub>RuTPP compounds. In all cases, the first and second oxidation events were attributed to the reversible oxidation of the Ru<sup>II</sup> center followed by the TPP(2-)/TPP(1-) process, with the further isocyanoazulene-based oxidations occurring at higher potentials. The stepwise reduction of the title compounds involves the axial isocyanoazulene ligands. Spectroelectrochemical and chemical oxidation methods were used to elucidate the spectroscopic signatures of the [(RNC)<sub>2</sub>RuTPP]<sup>n+</sup> ( $n = 1, 2$ ) species in solution. DFT and TDDFT calculations were employed to correlate the spectroscopic and redox properties of (2-CNaz)<sub>2</sub>RuTPP and (6-CNaz)<sub>2</sub>RuTPP with the electronic structures of these complexes.

## EXPERIMENTAL SECTION

**Materials.** All commercial reagents were ACS grade and were used without further purification. All reactions were performed under a dry argon atmosphere within flame-dried glassware. Toluene was distilled over sodium metal. Dichloromethane and hexanes were distilled over CaH<sub>2</sub>. Tetrabutylammonium tetrakis(pentafluorophenyl)borate (TFAB, (NBu<sub>4</sub>)[B(C<sub>6</sub>F<sub>5</sub>)<sub>4</sub>]),<sup>56</sup> 2-isocyanoazulene (2-CNaz),<sup>26</sup> and 6-isocyanoazulene (6-CNaz)<sup>26</sup> were prepared according to the published procedures.

**Synthetic Work. Synthesis of (2-CNaz)<sub>2</sub>RuTPP.** Commercially available (OC)RuTPP (0.16 g, 0.21 mmol) was added to a solution of the 2-CNaz ligand (0.20 g, 1.3 mmol) in 20 mL of the toluene/CH<sub>2</sub>Cl<sub>2</sub> (1/1, v/v) mixture under an argon atmosphere. The reaction mixture was stirred for 2 h at room temperature. The solvent was then removed under reduced pressure. The resulting solid was washed several times with hexanes, water, and dried under vacuum. Yield: 0.13 g (59%). Anal. Calcd for C<sub>66</sub>H<sub>42</sub>N<sub>6</sub>Ru·H<sub>2</sub>O: C, 76.36; H, 4.27; N, 8.09. Found: C, 76.01; H, 4.22; N, 7.90. <sup>1</sup>H NMR (300 MHz, CDCl<sub>3</sub>, peak assignments were deduced with the aid of 2D COSY):  $\delta$  8.55 (s, 8H,  $\beta$ -pyrrole), 8.19 (m, 8H, *m*-Ph), 7.67 (m, 12H, *o*-Ph, *p*-Ph), 7.65 (m, 4H, H<sup>4,8</sup>, C<sub>10</sub>H<sub>7</sub>NC), 7.32 (t, 2H, H<sup>6</sup>, C<sub>10</sub>H<sub>7</sub>NC, <sup>3</sup>J<sub>H-H</sub> = 9.8 Hz), 6.91 (t, H<sup>5,7</sup>, C<sub>10</sub>H<sub>7</sub>NC, <sup>3</sup>J<sub>H-H</sub> = 9.8 Hz), 5.32 (s, 4H, H<sup>1,3</sup>, C<sub>10</sub>H<sub>7</sub>NC) ppm. IR (KBr):  $\nu$ (NC) 2067 cm<sup>-1</sup>. HRMS (APCI-TOF, positive ions mode) calcd for C<sub>66</sub>H<sub>42</sub>N<sub>6</sub>Ru: 1020.2527. Found: 1020.2520 [M]<sup>+</sup>.

**Synthesis of (6-CNaz)<sub>2</sub>RuTPP.** Commercially available (OC)RuTPP (0.10 g, 0.13 mmol) was added to a solution of the 6-CNaz ligand (0.15 g, 0.99 mmol) in 50 mL of the toluene/CH<sub>2</sub>Cl<sub>2</sub> (1/1, v/v) mixture under an argon atmosphere. The reaction mixture was stirred for 2 h at room temperature. The solvent was then removed under reduced pressure. The resulting solid was washed several times with benzene-hexanes and dried under vacuum. Yield: 0.13 g (65%). Anal. Calcd for C<sub>66</sub>H<sub>42</sub>N<sub>6</sub>Ru·C<sub>6</sub>H<sub>6</sub>: C, 78.74; H, 4.40; N, 7.65. Found: C, 78.39; H, 4.67; N, 7.74. <sup>1</sup>H NMR (300 MHz, CDCl<sub>3</sub>, peak assignments were deduced with the aid of 2D COSY):  $\delta$  8.58 (s, 8H,  $\beta$ -pyrrole), 8.18 (m, 8H, *m*-Ph), 7.66 (m, 12H, *o*-Ph, *p*-Ph), 7.63 (t, H<sup>2</sup>, C<sub>10</sub>H<sub>7</sub>NC, <sup>3</sup>J<sub>H-H</sub> = 3.7 Hz), 7.40 (d, 4H, H<sup>4,8</sup>, C<sub>10</sub>H<sub>7</sub>NC, <sup>3</sup>J<sub>H-H</sub> = 10.7 Hz), 7.04 (d, 4H, H<sup>1,3</sup>, C<sub>10</sub>H<sub>7</sub>NC, <sup>3</sup>J<sub>H-H</sub> = 3.7 Hz), 4.59 (d, 4H, H<sup>5,7</sup>, C<sub>10</sub>H<sub>7</sub>NC, <sup>3</sup>J<sub>H-H</sub> = 10.7 Hz). IR (KBr):  $\nu$ (CN) 2061 cm<sup>-1</sup>. HRMS (APCI-TOF, positive ions mode) calcd for C<sub>66</sub>H<sub>42</sub>N<sub>6</sub>Ru: 1020.2527. Found: 1020.2525 [M]<sup>+</sup>.

**Instrumentation.** A Bruker Avance NMR instrument was used to acquire <sup>1</sup>H and 2D COSY NMR spectra at 300 MHz. The <sup>1</sup>H NMR spectra are referenced to the residual CHCl<sub>3</sub> solvent resonance, and the chemical shifts are reported in parts per million (ppm). All UV-vis data were obtained on a JASCO-720 spectrophotometer at room temperature. JASCO V-1500 and OLIS DCM 17 CD spectropolarimeters with a 1.1 T electro- or 1.4 T DeSa permanent magnet were used to obtain all

MCD data. The FTIR data were obtained on a PerkinElmer FTIR spectrometer Spectrum 100 at room temperature with solid samples dispersed in KBr pellets. Electrochemical measurements were conducted using a CHI-620C electrochemical analyzer employing the three-electrode scheme. Carbon or platinum working, platinum auxiliary, and Ag/AgCl pseudoreference electrodes were used in a 0.05 M solution of TFAB in  $\text{CH}_2\text{Cl}_2$ . The redox potentials are referenced to the  $\text{FcH}/\text{FcH}^+$  couple using decamethylferrocene as an internal standard. Spectroelectrochemical data were collected using a custom-made 1 mm cell, a working electrode made of platinum mesh, and a 0.15 M solution of TFAB in  $\text{CH}_2\text{Cl}_2$ . High-resolution APCI mass spectra were recorded using a Bruker MicrOTOF-III system for samples dissolved in THF. Elemental analyses were performed by Atlantic Microlab, Inc. in Atlanta, Georgia.

**DFT Computational Details.** All computations were performed using the Gaussian 09 software package running under UNIX OS.<sup>57</sup> Molecular orbital contributions were compiled from single-point calculations using the QMForge program.<sup>58</sup> All geometries were optimized using B3LYP exchange-correlation functional and full-electron double- $\zeta$  quality basis set (DGDZVP) for all atoms.<sup>59</sup> Frequencies were calculated for all optimized geometries in order to ensure that final geometries represent minima on the potential energy surface. In all single-point calculations, the M06 exchange-correlation functional<sup>45</sup> was used. TDDFT calculations were conducted for the first 80 excited states in order to ensure that all charge transfer (CT) and  $\pi$ - $\pi^*$  transitions of interest between 300 and 800 nm were accounted for. Solvent effects were modeled using the polarized continuum model approach.

**CASSCF Calculation Details.** The vertical excitation energy ( $S_0 \rightarrow S_1$ ) and its oscillator strength from the first singlet ground electronic state ( $S_0$ ) to the first excited electronic state ( $S_1$ ) were calculated at the expanded multiconfigurational quasi-degenerate perturbation theory (XMC-QDPT2) level using the def2-TZVP basis set and effective core-potential for ruthenium (RU-ECP-28,4).<sup>59,60,61</sup> The state averaged complete active space self-consistent field (SA-CASSCF) consisted of 16 electrons in 12 molecular orbitals. The state averaging was performed at the lowest 2 singlet and 2 triplet states. The effective Hamiltonian included 35 states. The all-multireference calculations were carried out in Firefly software.<sup>62</sup> We chose the XMC-QDPT2 method because it was successfully applied for the excited-state electronic energy calculations for a variety of small and large molecules.<sup>63–66</sup>

**X-ray Crystallography.** Single crystals of  $(2\text{-CNAz})_2\text{RuTPP}$  and  $(6\text{-CNAz})_2\text{RuTPP}$  suitable for X-ray crystallographic analysis were obtained by slow evaporation from their toluene solutions. X-ray diffraction data were collected on a Rigaku RAPID II Image Plate system using graphite-monochromated radiation. Experimental data collection, cell refinement, reduction, and absorption correction were performed by CrystalClear-SM Expert 2.0 r12.<sup>67</sup> The structures were solved by Superflip.<sup>68</sup> The toluene solvent molecule in the X-ray structure of the  $(2\text{-CNAz})_2\text{RuTPP}$  complex was found to be severely disordered and was removed using the PLATON SQUEEZE procedure. All hydrogen atoms were placed in their geometrically expected positions. The isotropic thermal parameters of all hydrogen atoms were fixed to the values of the equivalent isotropic thermal parameters of the corresponding carbon atoms using riding model constraints so that  $U_{\text{iso}}(\text{H}) = 1.2U_{\text{eq}}(\text{C})$  for the hydrogen atoms. Both structures reported herein were completely refined via the full-matrix least-squares method using the Crystals for Windows or SHELXTL program. Complete crystallographic information is available.

**Selected Crystal Data for  $(6\text{-CNAz})_2\text{RuTPP}$ :** FW 1020.12, Mo  $K\alpha$  radiation ( $\lambda = 0.71073 \text{ \AA}$ ) at 123 K, monoclinic, space group  $C2/c$ ,  $a = 23.455(2)$ ,  $b = 12.6158(8)$ ,  $c = 19.111(3) \text{ \AA}$ ,  $\alpha = 90^\circ$ ,  $\beta = 111.223(9)^\circ$ ,  $\gamma = 90^\circ$ ,  $V = 5271.6(10) \text{ \AA}^3$ ,  $Z = 4$ ,  $\mu = 0.345 \text{ mm}^{-1}$ , 9405 reflections ( $2982, I > 2.0/\sigma(I)$ ), parameters 715,  $\theta_{\text{max}} = 25.027$ ; final  $R_1 = 0.0711$ ,  $R_w = 0.1950$ . The toluene solvent molecule was removed using the program PLATON SQUEEZE.<sup>69</sup> The structure was refined by full-matrix least-squares refinement on  $F^2$  using SHELXL-2014/7<sup>70</sup> and the user interface ShelXle.<sup>71</sup> Additional crystallographic information may be found in CCDC-1902218.

**Selected Crystal Data for  $(2\text{-CNAz})_2\text{RuTPP}$ :** FW 1020.31, Cu  $K\alpha$  radiation ( $\lambda = 1.54187 \text{ \AA}$ ) at 123 K, monoclinic, space group  $P2_1/c$ ,  $a = 23.4732(17)$ ,  $b = 12.9276(2)$ ,  $c = 19.052(4) \text{ \AA}$ ,  $\alpha = 90^\circ$ ,  $\beta = 112.963(8)^\circ$ ,  $\gamma = 90^\circ$ ,  $V = 5323.2(11) \text{ \AA}^3$ ,  $Z = 4$ ,  $\mu = 2.790 \text{ mm}^{-1}$ , 9485 reflections ( $3734, I > 2.0/\sigma(I)$ ), parameters 330,  $\theta_{\text{max}} = 68.246$ ; Final  $R_1 = 0.1044$  [ $I > 2\sigma(I)$ ],  $R_w = 0.3674$  [ $I > 3\sigma(I)$ ]. The structure was refined by full-matrix least-squares refinement on  $F^2$  using CRYSTALS.<sup>72</sup> Additional crystallographic information can be found in CCDC-1902219.

## ■ ASSOCIATED CONTENT

### Supporting Information

The Supporting Information is available free of charge on the ACS Publications website at DOI: 10.1021/acs.inorgchem.9b01030.

Characterization data accompanying all synthetic work and computational details (PDF)

### Accession Codes

CCDC 1902218–1902219 contain the supplementary crystallographic data for this paper. These data can be obtained free of charge via [www.ccdc.cam.ac.uk/data\\_request/cif](http://www.ccdc.cam.ac.uk/data_request/cif), or by emailing [data\\_request@ccdc.cam.ac.uk](mailto:data_request@ccdc.cam.ac.uk), or by contacting The Cambridge Crystallographic Data Centre, 12 Union Road, Cambridge CB2 1EZ, UK; fax: +44 1223 336033.

## ■ AUTHOR INFORMATION

### Corresponding Authors

\*E-mail: [mbarybin@ku.edu](mailto:mbarybin@ku.edu).

\*E-mail: [victor.nemykin@umanitoba.ca](mailto:victor.nemykin@umanitoba.ca).

### ORCID

Gregory T. Rohde: 0000-0001-7787-8012

Rashid R. Valiev: 0000-0002-2088-2608

Victor N. Nemykin: 0000-0003-4345-0848

### Present Address

<sup>¶</sup>University of California—Irvine, 1102 Natural Sciences 2, Irvine, CA 92617, USA.

### Notes

The authors declare no competing financial interest.

## ■ ACKNOWLEDGMENTS

Generous support from the Minnesota Supercomputing Institute, NSERC, CFL, NSF (CHE-1464711 and MRI-0922366), University of Manitoba, and WestGrid Canada to V.N., and NSF (CHE-1214102 and CHE-1808120) to M.V.B. is greatly appreciated. V.R.R. thanks Svenska Kulturfonden, Grant No. 136102, and Academy of Finland, Grant No. 1315600.

## ■ REFERENCES

- (1) Barybin, M. V.; Meyers, J. J., Jr.; Neal, B. M. Renaissance of Isocyanoarenes as Ligands in Low-Valent Organometallics. In *Isocyanide Chemistry - Applications in Synthesis and Material Science*; Nenajdenko, V., Ed.; Wiley-VCH: Weinheim, Germany, 2012; pp 493–529.
- (2) Barybin, M. V. Nonbenzenoid aromatic isocyanides: New coordination building blocks for organometallic and surface chemistry. *Coord. Chem. Rev.* **2010**, *254*, 1240–1252.
- (3) Mahmudov, K. T.; Kukushkin, V. Yu.; Gurbanov, A. V.; Kinzhulov, M. A.; Boyarskiy, V. P.; da Silva, M. F. C. G.; Pombeiro, A. J.L. Isocyanide Metal Complexes in Catalysis. *Coord. Chem. Rev.* **2019**, *384*, 65–89.
- (4) Carpenter, A. E.; Mokhtarzadeh, C. C.; Ripatti, D. S.; Havrylyuk, I.; Kamezawa, R.; Moore, C. E.; Rheingold, A. L.; Figueroa, J. S. *Inorg. Chem.* **2015**, *54*, 2936–2944.

- (5) Hahn, F. E. The Coordination Chemistry of Multidentate Isocyanide Ligands. *Angew. Chem., Int. Ed. Engl.* **1993**, *32*, 650–665.
- (6) Qin, L.; Guan, X.; Yang, C.; Huang, J.-S.; Che, C.-M. Near-Infrared Phosphorescent Supramolecular Alkyl/Aryl-Iridium Porphyrin Assemblies by Axial Coordination. *Chem. - Eur. J.* **2018**, *24*, 14400–14408.
- (7) Nasri, S.; Brahmī, J.; Turowska-Tyrk, I.; Schulz, C. E.; Nasri, H. Synthesis, UV-visible and Mossbauer spectroscopic studies and molecular structure of the low-spin iron(II) Bis(tert-butyl isocyanide)-(5, 10, 15, 20-[4-(benzoyloxy)phenyl]porphyrin) coordination compound. *J. Organomet. Chem.* **2017**, *846*, 176–184.
- (8) Ohgo, Y.; Hoshino, A.; Okamura, T.; Uekusa, H.; Hashizume, D.; Ikezaki, A.; Nakamura, M. Metal-Porphyrin Orbital Interactions in Highly Saddled Low-Spin Iron(III) Porphyrin Complexes. *Inorg. Chem.* **2007**, *46*, 8193–8207.
- (9) Ohgo, Y.; Neya, S.; Uekusa, H.; Nakamura, M. An isocyanide probe for heme electronic structure: bis(tert-butylisocyanide) complex of diazaporphyrin showing a unique  $(d_{xy})^2(d_{xz}, d_{yz})^3$  ground state. *Chem. Commun.* **2006**, 4590–4592.
- (10) Zhang, L.; Fung, C. W.; Chan, K. S. Mechanistic studies of Si-CN and C-NC bond activation of silylnitriles and alkyl isonitriles by rhodium porphyrin radical: novel cyanide transfer. *Organometallics* **2006**, *25*, 5381–5389.
- (11) Yatsunyk, L. A.; Walker, F. A. NMR and EPR Spectroscopic and Structural Studies of Low-Spin,  $(d_{xz}, d_{yz})^4(d_{xy})^1$  Ground State Fe(III) Bis-tert-Butylisocyanide Complexes of Dodecasubstituted Porphyrins. *Inorg. Chem.* **2004**, *43*, 4341–4352.
- (12) Ikeue, T.; Ohgo, Y.; Saitoh, T.; Yamaguchi, T.; Nakamura, M. Factors Affecting the Electronic Ground State of Low-Spin Iron(III) Porphyrin Complexes. *Inorg. Chem.* **2001**, *40*, 3423–3434.
- (13) Walker, F. A.; Nasri, H.; Turowska-Tyrk, I.; Mohanrao, K.; Watson, C. T.; Shokhirev, N. V.; Debrunner, P. G.; Scheidt, W. R.  $\pi$ -Acid Ligands in Iron(III) Porphyrinates. Characterization of Low-Spin Bis(tert-butyl isocyanide)(porphyrinato)iron(III) Complexes Having  $(d_{xz}, d_{yz})^4(d_{xy})^1$  Ground States. *J. Am. Chem. Soc.* **1996**, *118*, 12109–12118.
- (14) Traylor, T. G.; Magde, D.; Taube, D.; Jongeward, K. Geminate recombination of iron(II) porphyrin with methyl-, tert-butyl-, and tosylmethyl- isocyanide, and 1-methylimidazole. *J. Am. Chem. Soc.* **1987**, *109*, 5864–5865.
- (15) Lim, Y.-M.; Park, H.-S.; Song, S.-H.; Park, C.-J.; Ryu, H.; Jee, J.-G.; Yang, H.-S. Synthesis and characterization of phthalocyaninatometal (PcM, M = Fe<sup>2+</sup>, Co<sup>2+</sup>) complexes with monodentate aromatic isocyanide ligands. *Bull. Korean Chem. Soc.* **1999**, *20*, 701–704.
- (16) Schmid, G.; Witke, E.; Schlick, U.; Knecht, S.; Hanack, M. Substituent effects in soluble phthalocyaninatoiron(II) complexes. *J. Mater. Chem.* **1995**, *5*, 855–859.
- (17) Janczak, J.; Kubiak, R.; Lisowski, J. Structural characterization and DFT calculation of the Fe-C coordinating bond in bis(tert-butyl isocyanide) iron(II) phthalocyanine. *J. Porphyrins Phthalocyanines* **2013**, *17*, 742–749.
- (18) Anderson, D. R.; Solntsev, P. V.; Rhoda, H. M.; Nemykin, V. N. How big is big? Separation by conventional methods, X-ray and electronic structures of positional isomers of bis-tert-butylisocyanide adduct of 2(3),9(10),16(17),23(24)-tetrachloro-3(2),10(9),17(16),24(23)-tetra(2,6-di-iso-propylphenoxy)-phthalocyaninato iron(II) complex. *J. Porphyrins Phthalocyanines* **2016**, *20*, 337–351.
- (19) Geiss, A.; Vahrenkamp, H. M( $\mu$ -CN)Fe( $\mu$ -CN)M' Chains with Phthalocyanine Iron Centers: Preparation, Structures, and Isomerization. *Inorg. Chem.* **2000**, *39*, 4029–4036.
- (20) Ryu, H.; Knecht, S.; Subramanian, L. R.; Hanack, M. Synthesis and properties of bridged phthalocyaninatoiron(II) complexes with bidentate aliphatic isocyanides. *Synth. Met.* **1995**, *72*, 289–296.
- (21) Keppeler, U.; Kobel, W.; Siehl, H. U.; Hanack, M. (Phthalocyaninato)iron(II)- and -ruthenium(II) compounds with isocyanides as axial ligands. *Chem. Ber.* **1985**, *118*, 2095–2104.
- (22) Vecchi, A.; Galloni, P.; Floris, B.; Dudkin, S. V.; Nemykin, V. N. Metallocenes meet porphyrinoids: Consequences of a "fusion". *Coord. Chem. Rev.* **2015**, *291*, 95–171.
- (23) Barybin, M. V.; Holovics, T. C.; Deplazes, S. F.; Lushington, G. H.; Powell, D. R.; Toriyama, M. First Homoleptic Complexes of Isocyanoferrrocene. *J. Am. Chem. Soc.* **2002**, *124*, 13668–13669.
- (24) Nemykin, V. N.; Dudkin, S. V.; Fathi-Rasekh, M.; Spaeth, A. D.; Rhoda, H. M.; Belosludov, R. V.; Barybin, M. V. Probing Electronic Communications in Heterotrinary Fe-Ru-Fe Molecular Wires Formed by Ruthenium(II) Tetraphenylporphyrin and Isocyanoferrrocene or 1,1'-Diisocyanoferrrocene Ligands. *Inorg. Chem.* **2015**, *54*, 10711–10724.
- (25) Nemykin, V. N.; Purchel, A. A.; Spaeth, A. D.; Barybin, M. V. Probing the Electronic Properties of a Trinuclear Molecular Wire Involving Isocyanoferrrocene and Iron(II) Phthalocyanine Motifs. *Inorg. Chem.* **2013**, *52*, 11004–11012.
- (26) Robinson, R. E.; Holovics, T. C.; Deplazes, S. F.; Powell, D. R.; Lushington, G. H.; Thompson, W. H.; Barybin, M. V. Five Possible Isocyanoozulenenes and Electron-Rich Complexes Thereof: A Quantitative Organometallic Approach for Probing Electronic Inhomogeneity of the Azulenene Framework. *Organometallics* **2005**, *24*, 2386–2397.
- (27) Maher, T. R.; Spaeth, A. D.; Neal, B. M.; Berrie, C. L.; Thompson, W. H.; Day, V. W.; Barybin, M. V. Linear 6,6'-Biazulenyl Framework Featuring Isocyanide Termini: Synthesis, Structure, Redox Behavior, Complexation, and Self-Assembly on Au(111). *J. Am. Chem. Soc.* **2010**, *132*, 15924–15926.
- (28) Applegate, J. C.; Okeowo, M. K.; Erickson, N. R.; Neal, B. M.; Berrie, C. L.; Gerasimchuk, N. N.; Barybin, M. V. First  $\pi$ -linker featuring mercapto and isocyano anchoring groups within the same molecule: synthesis, heterobimetallic complexation and self-assembly on Au(111). *Chem. Sci.* **2016**, *7*, 1422–1429.
- (29) Simonneaux, G.; Bondon, A. Isocyanides and Phosphines As Axial Ligands in Heme Proteins and Iron Porphyrin Models. In *Porphyrin Handbook*; Kadish, K. M., Smith, K. M., Guillard, R., Eds.; Academic Press: New York, 2000; Vol. 5, pp 299–322.
- (30) Galardon, E.; Le Maux, P.; Paul, C.; Poriel, C.; Simonneaux, G. <sup>1</sup>H-NMR and EPR studies of the electronic structure of low-spin ruthenium(III) isocyanide porphyrin complexes: unusual  $(d_{xz}, d_{yz})^4(d_{xy})^1$  configuration. *J. Organomet. Chem.* **2001**, *629*, 145–152.
- (31) Galardon, E.; Lukas, M.; Le Maux, P.; Toupet, L.; Roisnel, T.; Simonneaux, G. Bis[(R)-1-phenylethyl isocyanido](5,10,15,20-tetrakis[2,6-bis[(S)-2,2-dimethyl-1,3-dioxolan-4-ylmethoxy]-phenyl]porphyrin)ruthenium(II) at 110 K. *Acta Cryst., Section C* **2000**, *56*, 955–956.
- (32) Lee, F.-W.; Choi, M.-Y.; Cheung, K.-K.; Che, C.-M. Isocyanide ligation at ruthenium(II) complexes with chelating tertiary amine and porphyrin ligands. Structural and electrochemical studies. *J. Organomet. Chem.* **2000**, *595*, 114–125.
- (33) Maskasky, J. E.; Mooney, J. R.; Kenney, M. E. Iron(II) phthalocyanines as nuclear magnetic resonance shift reagents for amines. *J. Am. Chem. Soc.* **1972**, *94*, 2132–2133.
- (34) Choy, C. K.; Mooney, J. R.; Kenney, M. E. Selective iron(II) phthalocyanine and ruthenium(II) phthalocyanine shift reagents. *J. Magn. Reson.* **1979**, *35*, 1–12.
- (35) Hanack, M.; Vermehren, P. Soluble bisaxially substituted (phthalocyaninato)ruthenium complexes. *Chem. Ber.* **1991**, *124*, 1733–1738.
- (36) Fernandez, I.; Pregosin, P. S.; Albinati, A.; Rizzato, S.; Spichiger-Keller, U. E.; Nezel, T.; Fernandez-Sanchez, J. F. Solution NMR and X-ray structural studies on phthalocyaninatoiron complexes. *Helv. Chim. Acta* **2006**, *89*, 1485–1496.
- (37) Ona-Burgos, P.; Casimiro, M.; Fernandez, I.; Navarro, A. V.; Fernandez-Sanchez, J. F.; Carretero, A. S.; Gutierrez, A. F. Octahedral iron(II) phthalocyanine complexes: multinuclear NMR and relevance as NO<sub>2</sub> chemical sensors. *Dalton Trans.* **2010**, *39*, 6231–6238.
- (38) Nemykin, V. N.; Polshina, A. E.; Chernii, V. Y.; Polshin, E. V.; Kobayashi, N. Synthesis, properties and Mossbauer spectra of bisaxially co-ordinated iron(II) phthalocyanine low-spin complexes: the first

semi-quantitative explanation of the influence of the character of axial ligands on the spectral parameters. *Dalton* **2000**, 1019–1025.

(39) Nemykin, V. N.; Kobayashi, N.; Chernii, V. Y.; Belsky, V. K. Mossbauer, crystallographic, and density functional theoretical investigation of the electronic structure of bis-ligated low-spin iron(II) phthalocyanines. *Eur. J. Inorg. Chem.* **2001**, 2001, 733–743.

(40) Kobayashi, N.; Muranaka, A.; Mack, J. *Circular Dichroism and Magnetic Circular Dichroism Spectroscopy for Organic Chemists*; RSC: London, 2012; pp 1–216.

(41) Mason, W. R. *A Practical Guide to Magnetic Circular Dichroism Spectroscopy*; John Wiley & Sons, Inc.: Hoboken, NJ, 2007; pp 1–223.

(42) Waluk, J.; Michl, J. Perimeter model and magnetic circular dichroism of porphyrin analogs. *J. Org. Chem.* **1991**, 56, 2729–2735.

(43) Michl, J. Magnetic circular dichroism of cyclic  $\pi$ -electron systems. 3. Classification of cyclic  $\pi$  chromophores with a  $(4N + 2)$ -electron [n]annulene perimeter and general rules for substituent effects on the MCD spectra of soft chromophores. *J. Am. Chem. Soc.* **1978**, 100, 6819–6824.

(44) Sripathongnak, S.; Ziegler, C. J.; Dahlby, M. R.; Nemykin, V. N. Controllable and Reversible Inversion of the Electronic Structure in Nickel N-Confused Porphyrin: A Case When MCD Matters. *Inorg. Chem.* **2011**, 50, 6902–6909.

(45) Zhao, Y.; Truhlar, D. G. The M06 suite of density functionals for main group thermochemistry, thermochemical kinetics, noncovalent interactions, excited states, and transition elements: two new functionals and systematic testing of four M06-class functionals and 12 other functionals. *Theor. Chem. Acc.* **2008**, 120, 215–241.

(46) Becke, A. D. Density-functional exchange-energy approximation with correct asymptotic-behavior. *Phys. Rev. A: At., Mol., Opt. Phys.* **1988**, 38, 3098–3100.

(47) Perdew, J. P. Density-functional approximation for the correlation energy of the inhomogeneous electron gas. *Phys. Rev. B: Condens. Matter Mater. Phys.* **1986**, 33, 8822–8824.

(48) Tao, J. M.; Perdew, J. P.; Staroverov, V. N.; Scuseria, G. E. Climbing the density functional ladder: Nonempirical meta-generalized gradient approximation designed for molecules and solids. *Phys. Rev. Lett.* **2003**, 91, 146401.

(49) Becke, A. D. Density-functional thermochemistry. III. The role of exact exchange. *J. Chem. Phys.* **1993**, 98, 5648–5652.

(50) Yanai, T.; Tew, D.; Handy, N. A new hybrid exchange-correlation functional using the Coulomb-attenuating method (CAM-B3LYP). *Chem. Phys. Lett.* **2004**, 393, 51–57.

(51) Peverati, R.; Truhlar, D. G. Improving the Accuracy of Hybrid Meta-GGA Density Functionals by Range Separation. *J. Phys. Chem. Lett.* **2011**, 2, 2810–2817.

(52) Peverati, R.; Truhlar, D. G. Screened-exchange density functionals with broad accuracy for chemistry and solidstate physics. *Phys. Chem. Chem. Phys.* **2012**, 14, 16187.

(53) Xin, H.; Gao, X. Application of Azulene in Constructing Organic Optoelectronic Materials: New Tricks for an Old Dog. *ChemPlusChem* **2017**, 82, 945–956.

(54) Gouterman, M. Spectra of porphyrins. *J. Mol. Spectrosc.* **1961**, 6, 138–163.

(55) Gouterman, M.; Wagnière, G. H.; Snyder, L. C. Spectra of porphyrins. II. Four-orbital model. *J. Mol. Spectrosc.* **1963**, 11, 108–127.

(56) Barriere, F.; Geiger, W. E. Use of Weakly Coordinating Anions to Develop an Integrated Approach to the Tuning of  $\Delta E_{1/2}$  Values by Medium Effects. *J. Am. Chem. Soc.* **2006**, 128, 3980–3989.

(57) Frisch, M. J.; Trucks, G. W.; Schlegel, H. B.; Scuseria, G. E.; et al. *Gaussian 09*, revision D.1; Gaussian, Inc.: Wallingford, CT, 2009. For full citation, see the [Supporting Information](#).

(58) Tenderholt, A. L. *QMForge*, version 2.1; Stanford University: Stanford, CA.

(59) Godbout, N.; Salahub, D. R.; Andzelm, J.; Wimmer, E. Optimization of Gaussian-type basis sets for local spin density functional calculations. Part I. Boron through neon, optimization technique and validation. *Can. J. Chem.* **1992**, 70, 560–571.

(60) Granovsky, A. A. Extended multi-configuration quasi-degenerate perturbation theory: The new approach to multi-state multi-reference perturbation theory. *J. Chem. Phys.* **2011**, 134, 214113.

(61) Weigend, F.; Ahlrichs, R. Balanced basis sets of split valence, triple zeta valence and quadruple zeta valence quality for H to Rn: Design and assessment of accuracy. *Phys. Chem. Chem. Phys.* **2005**, 7, 3297–3305.

(62) Granovsky, A. A. *Firefly*, version 8.0.0; <http://classic.chem.msu.su/gran/firefly/index.html>.

(63) Valiev, R. R.; Cherepanov, V. N.; Baryshnikov, G. V.; Sundholm, D. First-principles method for calculating the rate constants of internal-conversion and intersystem-crossing transitions. *Phys. Chem. Chem. Phys.* **2018**, 20, 6121–6133.

(64) Minaev, B. F.; Valiev, R. R.; Nikonova, E. N.; Gadirov, R. M.; Solodova, T. A.; Kopylova, T. N.; Tel'minov, E. N. Kopylova. Computational and Experimental Investigation of the Optical Properties of the Chromene Dye. *J. Phys. Chem. A* **2015**, 119, 1948–1956.

(65) Valiev, R. R.; Fliegl, H.; Sundholm, D. Bicycloaromaticity and Baird-type bicycloaromaticity of dithienothiophene-bridged [34]-octaphyrins. *Phys. Chem. Chem. Phys.* **2018**, 20, 17705–17713.

(66) Valiev, R. R.; Fliegl, H.; Sundholm, D. Closed-shell paramagnetic porphyrinoids. *Chem. Commun.* **2017**, 53, 9866–9869.

(67) *Rigaku CrystalClear-SM Expert 2.0 r12*; Rigaku Corporation: Tokyo, Japan, 2011.

(68) Palatinus, L.; Chapuis, G. SUPERFLIP: A computer program for the solution of crystal structures by charge flipping in arbitrary dimensions. *J. Appl. Crystallogr.* **2007**, 40, 786–790.

(69) Spek, A. L. PLATON SQUEEZE: a tool for the calculation of the disordered solvent contribution to the calculated structure factors. *Acta Crystallogr., Sect. C: Struct. Chem.* **2015**, C71, 9–18.

(70) Sheldrick, G. M. A short history of SHELX. *Acta Crystallogr., Sect. A: Found. Crystallogr.* **2008**, A64, 112–122.

(71) Hübschle, C. B.; Sheldrick, G. M.; Dittrich, B. ShelXle: a Qt graphical user interface for SHELXL. *J. Appl. Crystallogr.* **2011**, 44, 1281–1284.

(72) Betteridge, P. W.; Carruthers, J. R.; Cooper, R. I.; Prout, K.; Watkin, D. J. CRYSTALS version 12: software for guided crystal structure analysis. *J. Appl. Crystallogr.* **2003**, 36, 1487.